sensors

MDPI

Article

Research on Joint-Angle Prediction Based on Artificial Neural Network for Above-Knee Amputees

Jianyu Yang, Guanchao Li, Xiaofei Zhao and Hualong Xie *

Department of Mechanical Engineering and Automation, Northeastern University, Shenyang 110004, China; jyyang@mail.neu.edu.cn (J.Y.); lgc202109@163.com (G.L.); zhaoxiaofei5@hikvision.com (X.Z.)
* Correspondence: hlxie@mail.neu.edu.cn

Abstract: In the current study, our research group proposed an asymmetric lower extremity exoskeleton to enable above-knee amputees to walk with a load. Due to the absence of shank and foot, the knee and ankle joint at the amputation side of the exoskeleton lack tracking targets, so it is difficult to realize the function of assisted walking when going up and downstairs. Currently, the use of lower-limb electromyography to predict the angles of lower limb joints has achieved remarkable results. However, the prediction effect was poor when only using electromyography from the thigh. Therefore, this paper introduces hip-angle and plantar pressure signals for improving prediction effect and puts forward a joint prediction method of knee- and ankle-joint angles by electromyography of the thigh, hip-joint angle, and plantar pressure signals. The generalized regression neural network optimized by the golden section method is used to predict the joint angles. Finally, the parameters (the maximum error, the Root-Mean-Square error (*RMSE*), and correlation coefficient (γ)) were calculated to verify the feasibility of the prediction method.

Keywords: asymmetric lower extremity exoskeleton; electromyographic signals; artificial neural network; joint-angle prediction; going up and downstairs

Citation: Yang, J.; Li, G.; Zhao, X.; Xie, H. Research on Joint-Angle Prediction Based on Artificial Neural Network for Above-Knee Amputees. *Sensors* **2021**, *21*, 7199. https://doi.org/10.3390/s21217199

Academic Editor: M. Osman Tokhi

Received: 25 September 2021
Accepted: 19 October 2021
Published: 29 October 2021

1. Introduction

The number of patients with lower-limb disabilities has been rapidly increasing. Most of them have lost their lower limbs due to natural disasters, traffic accidents and wars [1,2]. Currently, prostheses are the most significant tools to compensate for the walking function of lower-limb amputees [3–7]. However, most prostheses on the market, either passive or semiactive, cannot realize the joints' active swinging, and thus fail to achieve assisted walking [8]. The lower extremity exoskeleton (LEE) assists amputees in rehabilitation training [9–11]. The LEE wearer can move around safely and flexibly for a long time at high speed under heavy load. The LEE has been widely used in marching, weight-bearing combat, and medical rehabilitation proposes [12,13].

Considering the desire of above-knee amputees to walk like healthy persons and even walk with a load, as shown in Figure 1, our research group designs an asymmetric LEE [14] with two working modes, including the active mode and the semiactive mode. Under the active mode, the LEE motor provides a driving torque, enabling the wearer to walk with a load. When the prosthesis part is detached from the LEE, the prosthesis part can work as a normal prosthesis in the semiactive mode.

There are many problems that need to be solved in the research on asymmetric LEE. Additionally, this paper focuses on the study of how the prosthesis can better assist the patient to go upstairs and downstairs, when the prosthesis is disassembled from the LEE and worn on the patient's residual limb to work alone. Therefore, it is important to obtain the joint angle of human lower limbs when controlling the prosthesis. Previous researchers have used electromyography (EMG) for joint-angle prediction. Chen et al. [15] and Zhang et al. [16] used the BP network to map the relationship between joint angles and EMG signals. Du et al. [17] used the least-squares extreme learning-machine algorithm

based on the golden section to establish a nonlinear prediction model between surface electromyography (sEMG) and lower-limb joint angle. However, they used the EMG signals from the thigh and the calf. They did not evaluate the corresponding relationship between joint angles and EMG signals when walking up and downstairs, nor did they use the plantar pressure signals for the joint-angle prediction. Gaudet et al. [18] achieved the classification of upper limb phantom movements in transhumeral amputees using electromyographic and kinematic features. Previous scholars have proven that sEMG signals of residual limbs of amputation patients could be used for motion intention recognition, which verified the feasibility of sEMG signals in motion control for the prosthesis [19–21]. The muscles on the thigh stump could also be activated when amputee moves. The weak signals could be amplified and then be filtered, therefore the effective function could be obtained. Because of the lack of above-knee amputees to help with our research, the volunteers in this work were healthy people. A previous paper [22] demonstrates the feasibility and applicability of using healthy human body signals to study amputees. sEMG signals collected in the experiment were all from the muscles on the thigh related to the hip joint swing, to simulate the case of above-knee amputees as much as possible. In this study, we found that the existing prediction methods based on angle and sEMG signals are slightly less accurate during the support period. Considering that the plantar pressure signal is closely related to the support period and has the characteristics of periodic changes, this natural repeatability was exploited to improve the accuracy of the estimation method, which is the novelty of this paper. The research content is shown in Figure 2. This paper is organized as follows. Section 2 starts by the establishment of a data acquisition system, the collection and processing of sEMG, joint angle and plantar pressure signals. It ends with the design of an artificial neural network that focus on the angle estimation. The obtained results are presented and analyzed in Section 3, while Section 4 discusses them. Conclusions are presented in Section 5.

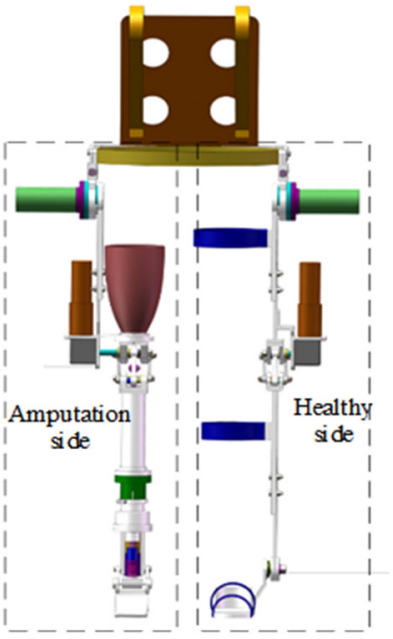

Figure 1. Asymmetric lower limb exoskeleton.

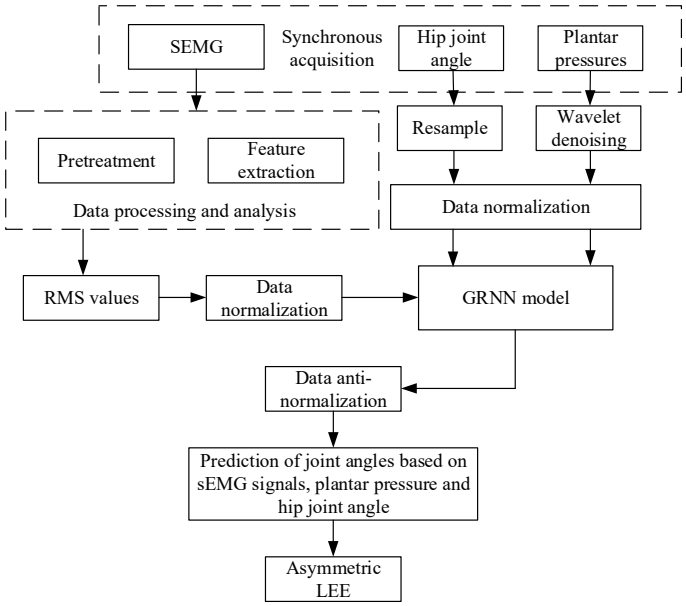

Figure 2. Flow chart of joint-angle prediction.

2. Experiment and Methods

2.1. Data Acquisition System Establishment

To obtain EMG, joint angle, and plantar pressure signals synchronously, a data acquisition system was designed in this paper, as shown in Figure 3. This system was composed of thin-film pressure sensors, EMG sensors, six-axis angle sensors, a data acquisition card, an ARDUINO MEGA microcontroller, etc. To acquire the pressure signals under the big toe, forefoot, and heel in real-time, three thin-film pressure sensors were placed in an insole, as shown in Figure 4. Due to the limitation of sensors, different signals were collected by different devices. In order to ensure data synchronization, we figured out a way to solve the problem of synchronization. Angle signals and plantar pressure signals were collected by Arduino synchronously, while sEMG signals and plantar pressure signals were collected by the data acquisition card synchronously. During the data acquisition process, plantar pressure signals were the same. Pressure signal data were generated simultaneously although they were collected by different equipment. Based on the pressure signals, the angle and the sEMG signals could be time-synchronized. The frequency of sEMG collected by the data acquisition card was very stable. Additionally, the effective part of the sEMG signal was mainly distributed in the range of 0–500 Hz. According to the sampling theorem, the frequency is finally set as 2000 Hz. Band-pass filtering was performed on sEMG signals to remove interference, and the root-mean-square eigenvalues were extracted at every 20 data points. So, the final frequency of processed sEMG signals is 100 Hz. The frequency of raw plantar pressure is also 2000 Hz. Then, the averages of plantar pressure signals were extracted as the eigenvalues of pressure data every 20 points. After processing, the frequency of the pressure signal is 100 Hz. In the process of collecting angle signals, due to equipment problems, the sampling frequency of the angle signal was affected. In order to ensure that the frequency of the angle signal was consistent with the sEMG and pressure signal, the angle signal was first fitted and then resampled, and the final frequency was 100 Hz. As a result, angle, pressure, and sEMG signals could be frequency-synchronized.

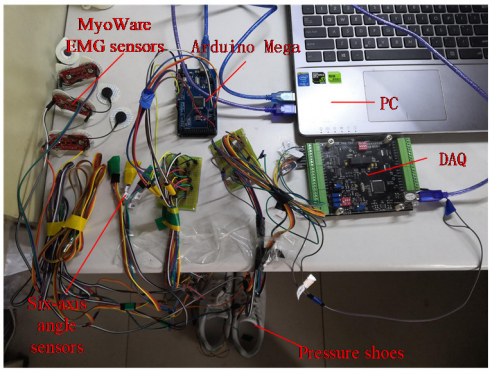

Figure 3. Designed data acquisition system.

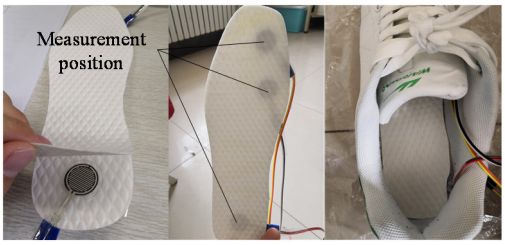

Figure 4. Position of pressure sensors.

2.2. Data Acquisition

The data in this paper were collected from three healthy males (aged 25 ± 2 years). Each one walked upstairs and downstairs 20 times. Before the experiment, no vigorous exercise was done by the technicians, and alcohol was used to clear the skin and increase the conductance. The EMG signals were measured in the rectus femoris, biceps femoris and semitendinosus muscles of the thigh. Furthermore, the angle signals and plantar pressure signals were simultaneously acquired. As examples, two data acquisition photos are shown in Figure 5.

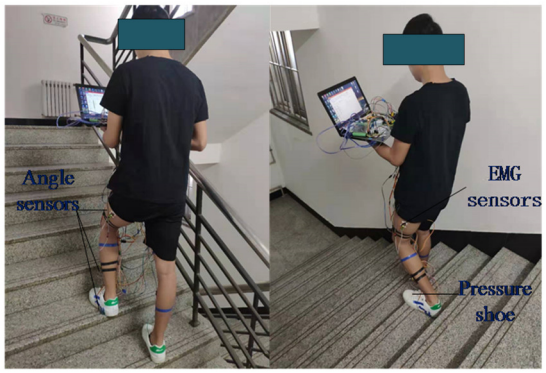

Figure 5. Data acquisition process.

2.3. Surface EMG Signal Preprocessing

According to the Nyquist sampling theorem, the sampling frequency of EMG signals in this paper was set at 2000 Hz. The raw EMG signals were then collected, and signals were filtered by a bandpass filter with a frequency range of 20–500 Hz. The parameters of filter is shown in Table 1. One of the filtered signals is shown in Figure 6.

Table 1. Main parameters of band-pass filter.

Parameters	Value
Pass-band Upper Cutoff Frequency (Hz)	20
Pass-band Lower Cutoff Frequency (Hz)	500
Pass-band Maximum Attenuation (dB)	3
Stop-band Upper Cutoff Frequency (Hz)	10
Stop-band Lower Cutoff Frequency (Hz)	570
Stop-band Minimum Attenuation (dB)	20

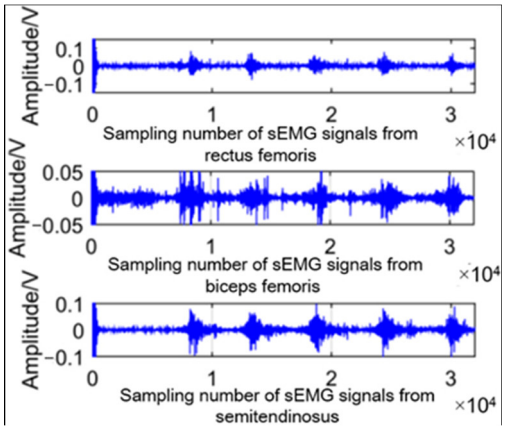

Figure 6. EMG signals in going upstairs procedure after band-pass filter.

Next, the characteristic values of sEMG signals that were filtered were extracted. There are many characteristic values, we selected the most commonly used Root Mean Square (*RMS*) that could contain the most useful information in the signal, as shown in Figure 7. *RMS* values were calculated every 20 data points by:

$$RMS = \sqrt{\frac{1}{N}\sum_{i=1}^{N} x(i)^2} \quad (1)$$

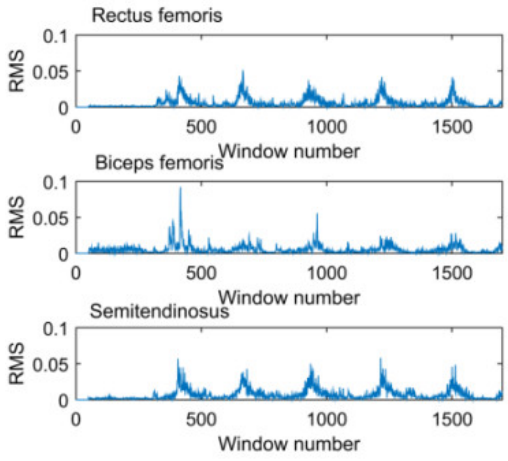

Figure 7. *RMS* of sEMG signals.

2.4. Joint-Angle Signal Processing

The angle signals were sampled twice to unite the sampling frequency of sEMG signals, so the final frequency of the angle was 100 Hz. In this paper, piecewise polynomial

curve fitting was used for resampling of joint-angle signals. Figure 8 shows one of the piecewise curve-fitting results during going up the stairs.

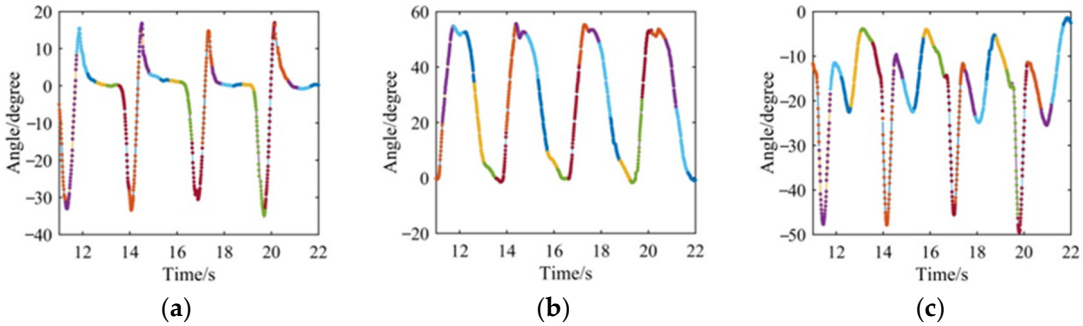

Figure 8. Piecewise curve-fitting results in going upstairs process. (**a**) Angle of hip joint; (**b**) Angle of knee joint; (**c**) Angle of ankle joint.

2.5. Plantar Pressure Signal Processing

The plantar pressure signals were processed by taking the time windows because the pressure signal and sEMG signals were collected synchronously. Each window has 20 points, and the average value of the data in each window is calculated as the characteristic value of pressure signals. The raw plantar pressure signals and the characteristic values are shown in Figures 9 and 10, respectively.

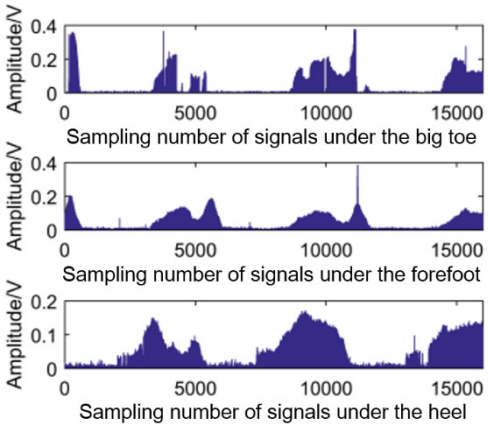

Figure 9. The raw plantar pressure signals.

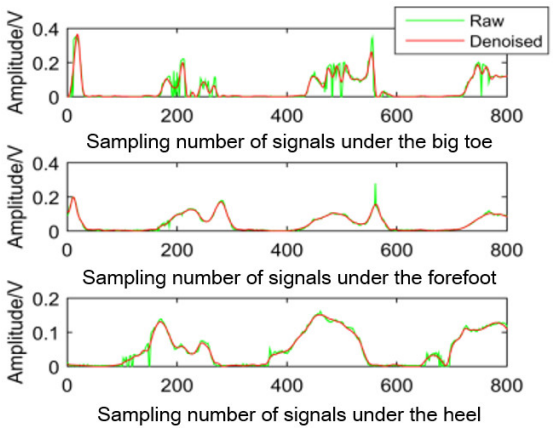

Figure 10. Characteristic values of plantar pressure signals.

2.6. GS-GRNN Network for Angle Estimation

In the machine-learning algorithm, the support vector machine (SVM) performs efficiently in pattern recognition [23,24]; however, it is not effective in dealing with nonlinear mapping problems. This paper used an artificial neural network to map the joint angles [25–27]. Generalized regression neural network (GRNN) is a network developed from radial basis function neural network, as shown in Figure 11.

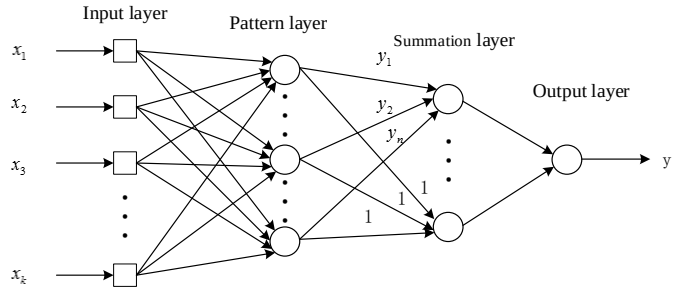

Figure 11. Structure of GRNN.

Suppose the joint probability density of random variable x and random variable y is f (x, y), and the observed value of x is X, then the regression of y relative to X is the prediction output of the neural network as follows:

$$\hat{Y}(X) = \frac{\sum_{i=1}^{n} Y_i \exp[-\frac{(X-X_i)^T(X-X_i)}{2\sigma^2}]}{\sum_{i=1}^{n} \exp[-\frac{(X-X_i)^T(X-X_i)}{2\sigma^2}]} \tag{2}$$

where $\hat{Y}$ is the prediction result of Y under the condition that the input is X, X_i and Y_i are the observed values of X and Y, n is the number of samples, σ is the smoothing factor $(\sigma > 0)$, $D_i^2 = (X - X_i)^T(X - X_i)$ is the square of Euclidean distance between X and X_i. The transfer function of the hidden layer is:

$$p_i = \exp[-\frac{(X - X_i)^T(X - X_i)}{2\sigma^2}] \tag{3}$$

The units in the summation layer are the denominator and numerator of Equation (2), respectively:

$$S_D = \sum_{i=1}^{n} P_i \tag{4}$$

$$S_N = \sum_{i=1}^{n} Y_i P_i \tag{5}$$

Therefore, the result of the output layer is:

$$\hat{Y} = \frac{S_N}{S_D} \tag{6}$$

The smoothing factor affects the network performance, which has a significant influence on the network. In this paper, the generalized regression neural network was optimized by golden section algorithm (GS-GRNN). The objective function is the mean square error between the predicted value Y_i of the joint angle and the measured value of Y:

$$E = \frac{1}{N}\sum_{i=1}^{N} (Y_i - Y)^2 \tag{7}$$

where N represents the number of predicted samples. The flow chart of the golden section algorithm is shown in Figure 12, where $\varphi(t)$ is the objective function, ε is the termination limit, and σ is the value range of (a, b).

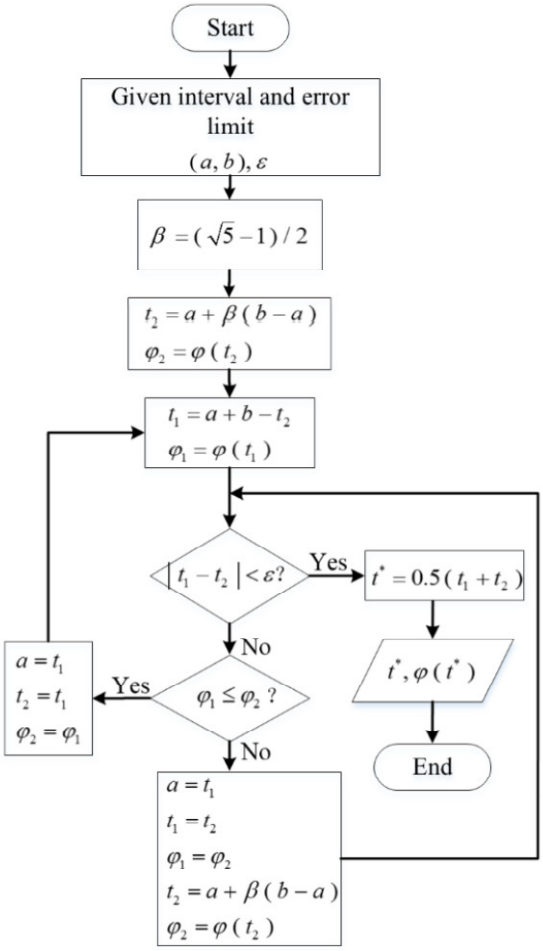

Figure 12. The flow chart of the golden section algorithm.

2.7. Data Normalization Processing

Before the training of an artificial neural network, the data was normalized to avoid singular sample data. In this paper, the data were normalized by:

$$x' = \frac{x - minA}{maxA - minA} \tag{8}$$

where x is the original data, x' is the corresponding value after normalization, $maxA$ is the maximum value set, and $minA$ is the minimum data set.

3. Analysis of Results

GS-GRNN was used to predict the joint angles during the going upstairs and downstairs processes. The inputs were EMG signals of the thigh (IN1), EMG signals and angle signals of the hip joint (IN2), EMG signals, angle signals of the hip joint and plantar pressure signals (IN3). The outputs were angle signals of the hip joint, knee joint, and ankle joint. Among them, one third of that data was used for validation and testing, and two thirds of that data was used for training. We take one set of experimental data during going upstairs and downstairs as examples. Figures 13–18 show the prediction results of each joint angle.

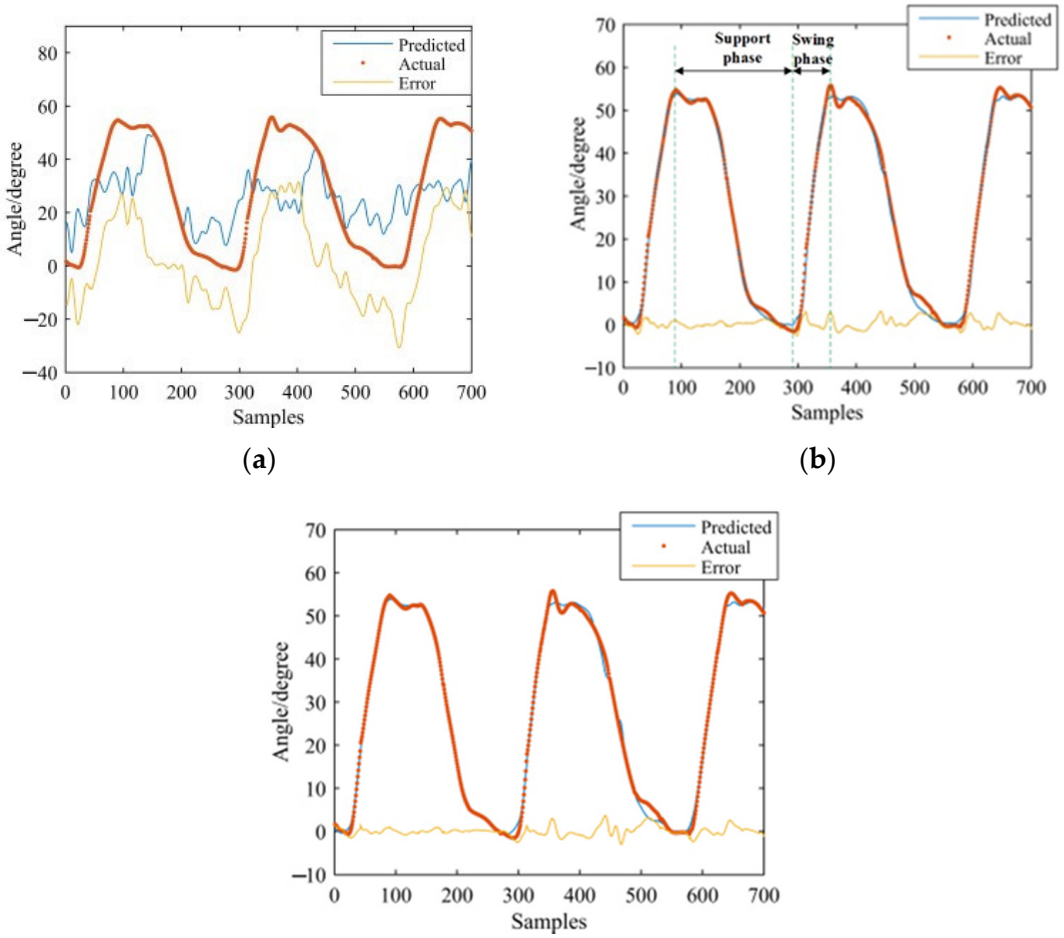

Figure 13. Prediction results of hip-joint angle in the going upstairs process. (**a**) Results of IN1; (**b**) Results of IN2; (**c**) Results of IN3.

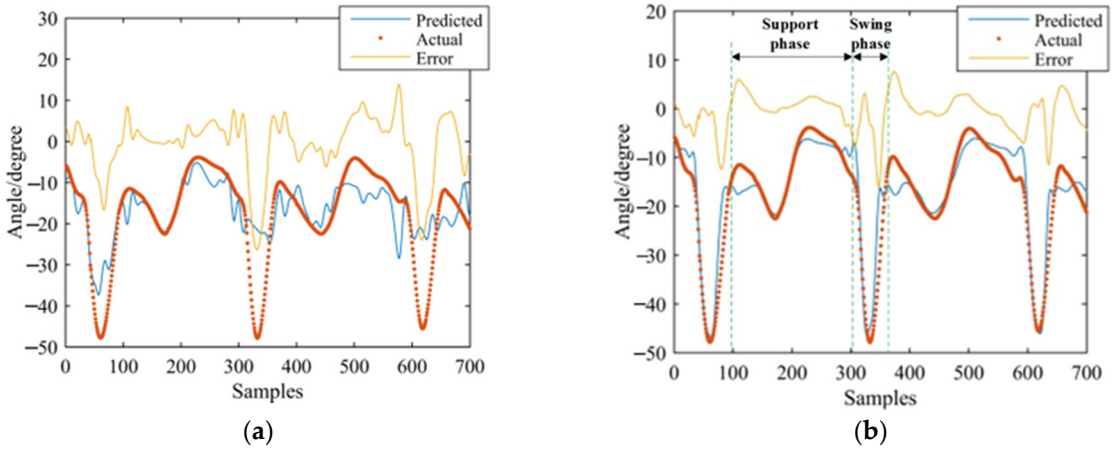

Figure 14. *Cont.*

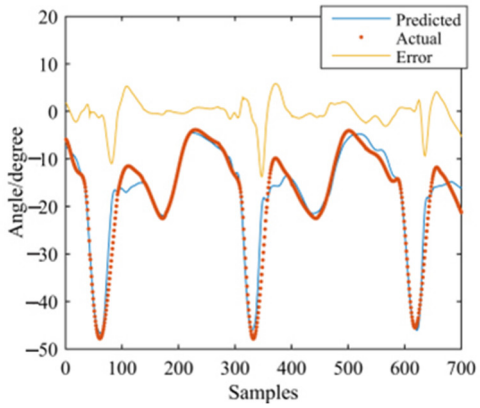

(**c**)

Figure 14. Prediction results of knee-joint angle in the going upstairs process. (**a**) Results of IN1; (**b**) Results of IN2; (**c**) Results of IN3.

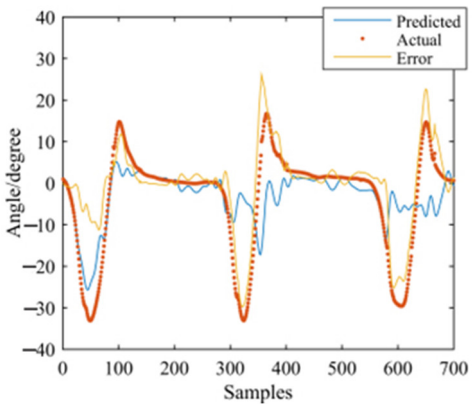

(**a**)

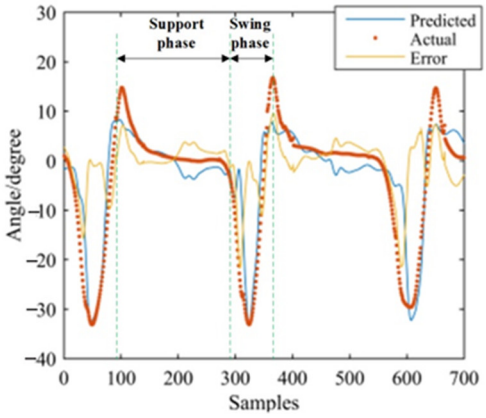

(**b**)

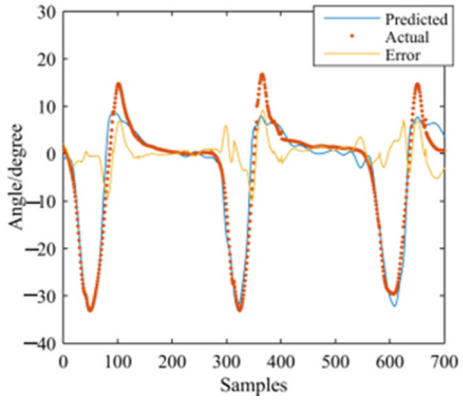

(**c**)

Figure 15. Prediction results of ankle-joint angle in the going upstairs process. (**a**) Results of IN1; (**b**) Results of IN2; (**c**) Results of IN3.

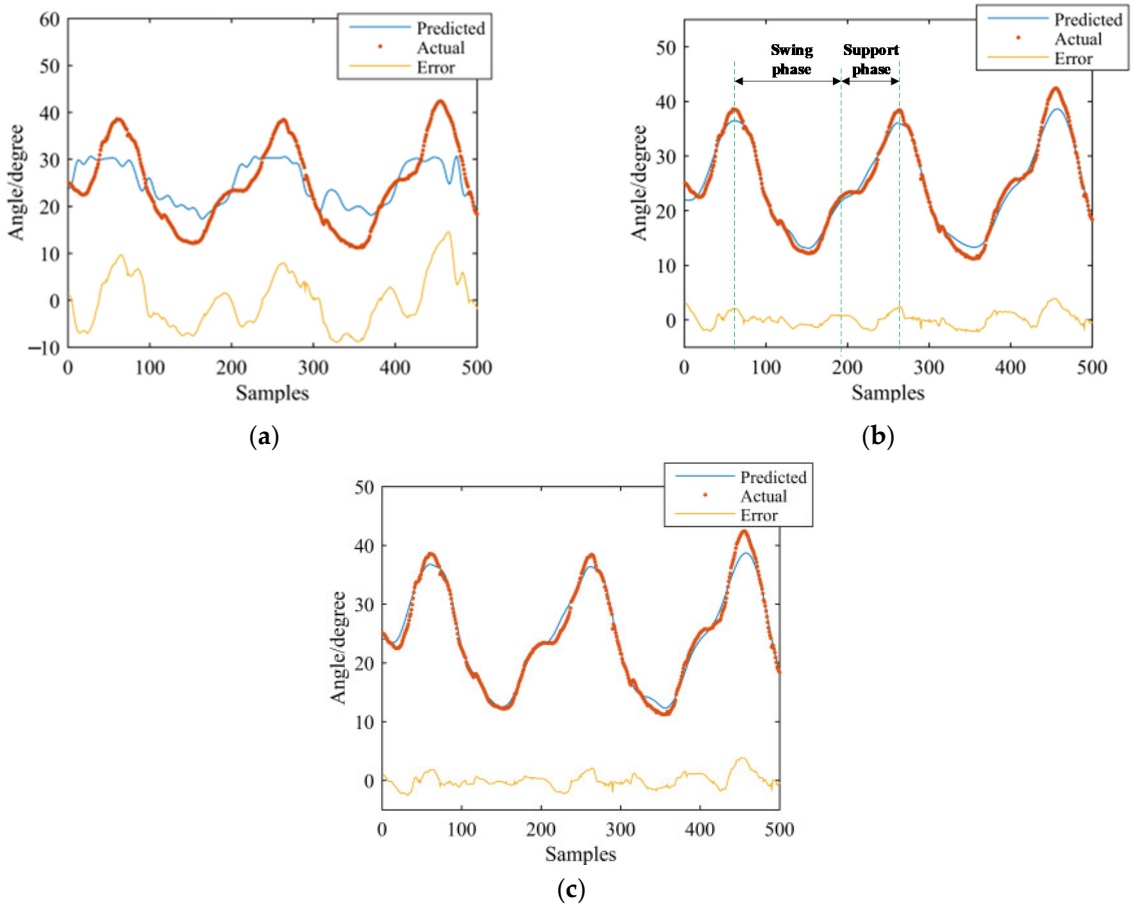

Figure 16. Prediction results of hip-joint angle in the going downstairs process. (**a**) Results of IN1; (**b**) Results of IN2; (**c**) Results of IN3.

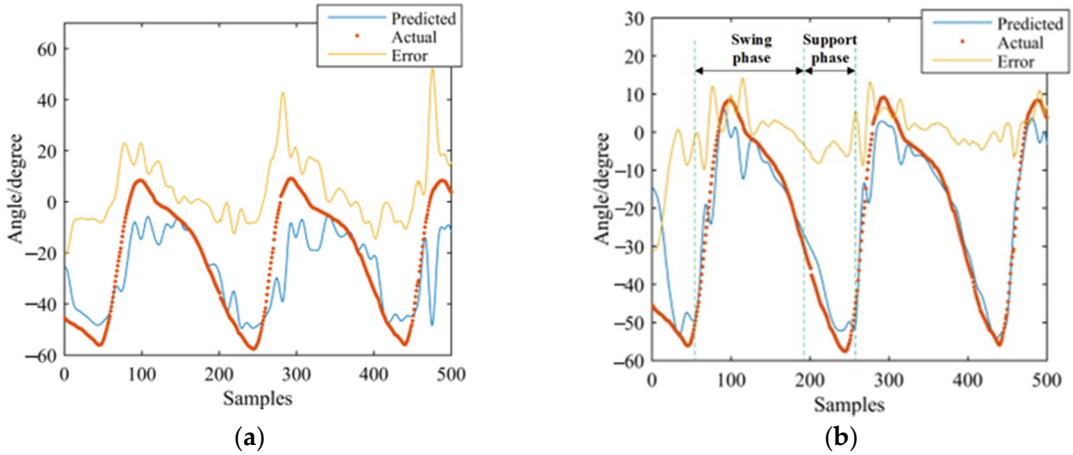

Figure 17. *Cont.*

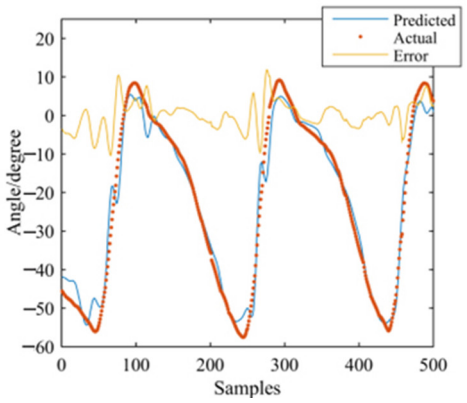

(**c**)

Figure 17. Prediction results of knee-joint angle in the going downstairs process. (**a**) Results of IN1; (**b**) Results of IN2; (**c**) Results of IN3.

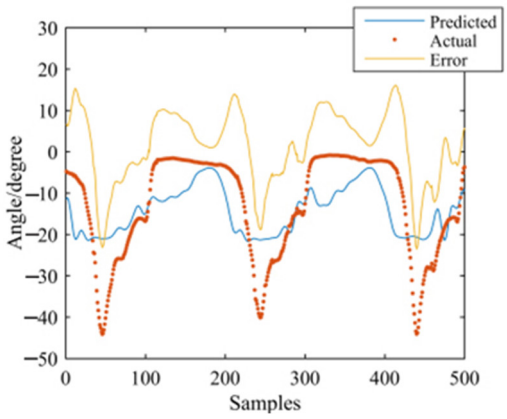

(**a**)

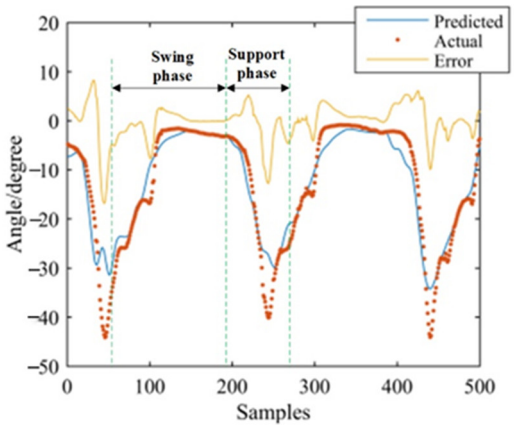

(**b**)

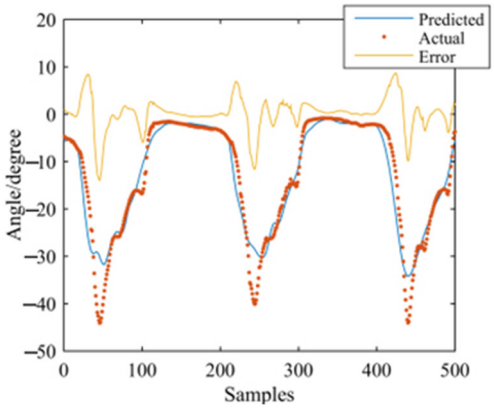

(**c**)

Figure 18. Prediction results of ankle-joint angle in the going downstairs process. (**a**) Results of IN1; (**b**) Results of IN2; (**c**) Results of IN3.

To further analyze the prediction results, the maximum error, the Root-Mean-Square error (*RMSE*), and correlation coefficient (γ) were calculated as shown in Figures 19–24.

$$RMSE = \sqrt{\frac{1}{N}\sum_{i=1}^{N}(x_i - y_i)^2} \quad (9)$$

$$\gamma = \frac{\frac{1}{N}\sum_{i=1}^{N}(x_i - \overline{x})(y_i - \overline{y})}{\sqrt{\frac{1}{N}\sum_{i=1}^{N}(x_i - \overline{x})^2}\sqrt{\frac{1}{N_a}\sum_{i=1}^{N_a}(y_i - \overline{y})^2}} \tag{10}$$

where, x_i is the predicted value, y_i is the actual value, N is the number of samples, $\overline{x}$ and $\overline{y}$ are the mean values of the predicted value, and the actual measured value, respectively.

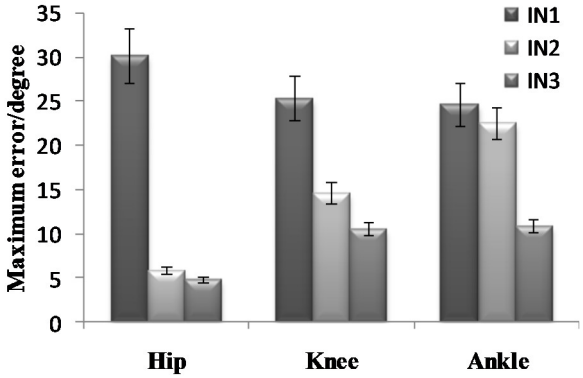

Figure 19. Maximum error of the prediction results in the going upstairs process.

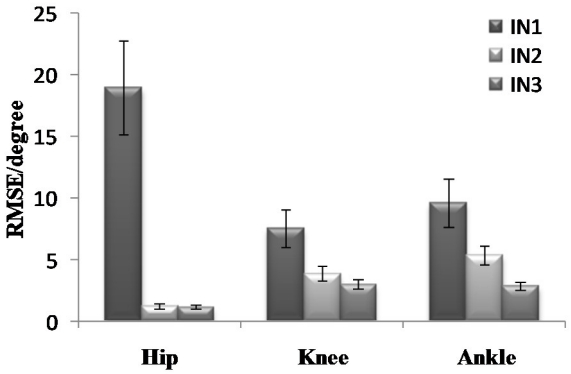

Figure 20. *RMSE* of the prediction results in the going upstairs process.

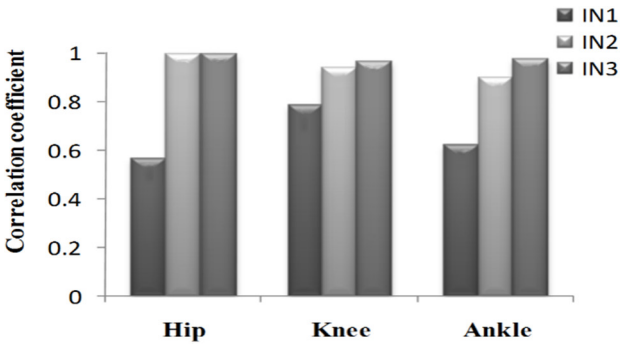

Figure 21. Correlation coefficient of the prediction results in the going upstairs process.

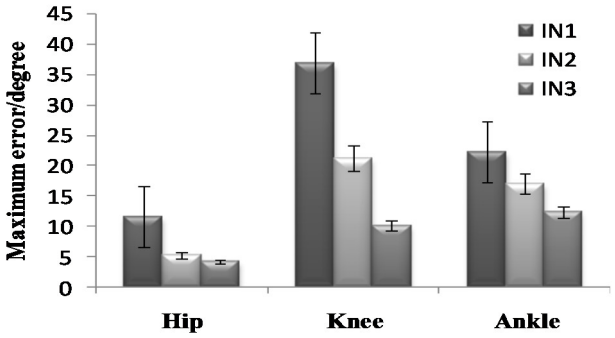

Figure 22. Maximum error of the prediction results in the going downstairs process.

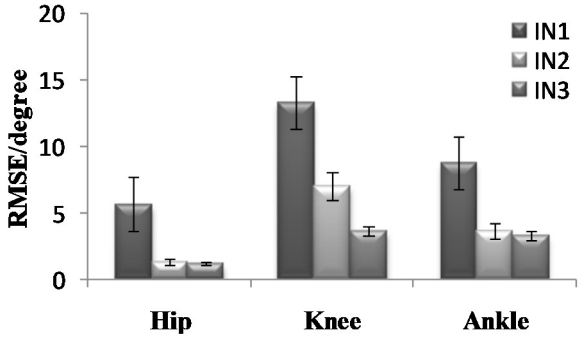

Figure 23. *RMSE* of the prediction results in the going downstairs process.

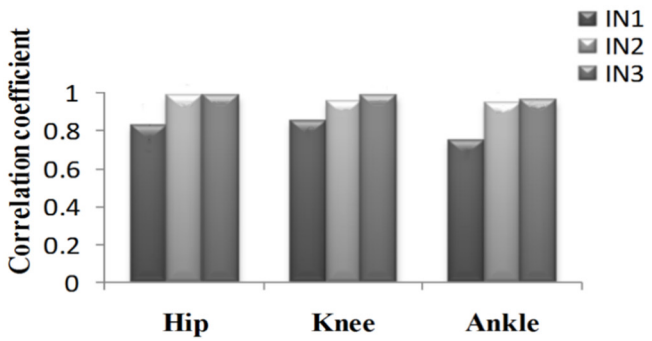

Figure 24. Correlation coefficient of the prediction results in the going downstairs process.

4. Discussion

We found that the addition of plantar pressure signals can effectively improve the prediction effect of knee and ankle angles. The prediction effect was the best when imputing EMG signals, hip-joint angle signals, and plantar pressure signals synchronized with each other. During going upstairs, the correlation coefficients of the hip-, knee-, and ankle-joint angles can reach 0.9986, 0.9649 and 0.9771, respectively. The root-mean-square errors are 1.1530, 3.0077 and 2.8407, respectively. During going downstairs, the correlation coefficients can reach 0.9921, 0.9893 and 0.9635, and the root-means-square errors are 1.1725, 3.5974 and 3.3239, respectively. As discussed in the results above, based on the GS-GRNN network, lower-limb-joint angle prediction is realized in this paper. When only the hip-joint angle was used as an input, low accuracy and high error were achieved. When the input included angle and EMG signals, the accuracy and the correlation coefficients were significantly improved. When the angle, EMG, and plantar pressure signals were simultaneously imported into GRNN together, the accuracy and the correlation coefficient were further improved. The addition of plantar pressure signals expands the sample data. Generally, when the input signals and data samples increase, the neural network becomes more trained, and more accurate results could be obtained.

5. Conclusions

This paper optimizes the joint-angle prediction method by integrating hip-joint angle signals, sEMG signals, and plantar pressure signals to solve the problem of online gait planning of asymmetric lower extremity exoskeletons. Furthermore, each joint follows a periodic trajectory in the function of the gait phase. Therefore, the plantar pressure signal that contains gait phase information improves this work and enriches the motion information of the input data, improving the prediction accuracy.

GS-GRNN used for joint-angle prediction performs well in this paper. The prediction results confirmed the optimization method's feasibility, and finally, a joint-angle prediction method for above-knee amputees was developed, which provided a favorable reference for LEE's movement control.

To ensure the patients' safety, we have been recently practicing these techniques on healthy people. However, with the development of research, we will try to recruit amputees so that we can to make this algorithm more adaptable.

Author Contributions: J.Y. carried out the experiments. H.X. provided equipment for this study. G.L. processed the experiment data. X.Z. checked the expression and grammar of the article. All authors have read and agreed to the published version of the manuscript.

Funding: This research was funded by the National Science Foundation of China, grant number No.61803272 and the Fundamental Research Funds for the Central University of the Ministry of Education of China, grant number No.N 2103031.

Institutional Review Board Statement: The study was conducted according to the guidelines of the Declaration of Helsinki, and approved by the Institutional Review Board of Biological and Medical Ethics Committee of North-eastern University (EC-2021B018 and 1 September 2021).

Informed Consent Statement: Informed consent was obtained from all subjects involved in the study.

Data Availability Statement: Not applicable.

Conflicts of Interest: The authors declare no conflict of interest.

References

1. Zhou, T.Y.; Chen, Y.S. Communiqué on Major Statistics of the Second China National Sample Survey on Disability. *Chin. J. Rehabil. Theory Pract.* **2006**, *12*, 1013.
2. Tian, B.; Zhang, Y.; Qiu, Z.Y. Comparison and Analysis of Data Obtained in Two National Sampling Surveys of Disability. *Chin. J. Spec. Educ.* **2007**, *8*, 54–56.
3. Xie, H.L.; Xie, Y.; Li, F. Design, Modeling and Control of Bionic Knee in Artificial Leg. *Int. J. Comput. Commun. Control.* **2019**, *14*, 733–752. [CrossRef]
4. Tileylioglu, E.; Yilmaz, A. Application of neural based estimation algorithm for gait phases of above knee prosthesis. In Proceedings of the 2015 37th Annual International Conference of the IEEE Engineering in Medicine and Biology Society (EMBC), Milan, Italy, 25–29 August 2015.
5. Paskett, M.D.; Brinton, M.R.; Hansen, T.C.; George, J.A.; Tyler, S.D.; Christopher, C.D.; Gregory, A.C. Activities of daily living with bionic arm improved by combination training and latching filter in prosthesis control comparison. *J. NeuroEng. Rehabil.* **2021**, *18*, 45. [CrossRef] [PubMed]
6. Li, X.; Liu, Z.; Gao, X.; Zhang, J. Bicycling Phase Recognition for Lower Limb Amputees Using Support Vector Machine Optimized by Particle Swarm Optimization. *Sensors* **2020**, *20*, 6533. [CrossRef] [PubMed]
7. Ortiz-Catalan, M.; Hakansson, B.; Branemark, R. An osseointegrated human-machine gateway for long-term sensory feedback and motor control of artificial limbs. *Sci. Transl. Med.* **2014**, *6*, 257re6. [CrossRef] [PubMed]
8. Hong, G.U.; Li, W.D.; Li, J. State-of-the-art and Development of Intelligent Knee Prosthesis. *Chin. J. Rehabil. Theory Pract.* **2016**, *22*, 1080–1085.
9. Yang, W.; Zhang, J.; Zhang, S.; Yang, C. Lower Limb Exoskeleton Gait Planning Based on Crutch and Human-Machine Foot Combined Center of Pressure. *Sensors* **2020**, *20*, 7216. [CrossRef] [PubMed]
10. Dollar, A.M.; Herr, H. Lower Extremity Exoskeletons and Active Orthoses: Challenges and State-of-the-Art. *IEEE Trans. Robot.* **2008**, *24*, 144–158. [CrossRef]
11. Wu, Q.; Wu, H. Development, Dynamic Modeling, and Multi-Modal Control of a Therapeutic Exoskeleton for Upper Limb Rehabilitation Training. *Sensors* **2018**, *18*, 3611. [CrossRef] [PubMed]
12. Seung, H.H.; Dong, I.S.; Wan, S.K. Gait pattern generation algorithm for lower-extremity rehabilitation-exoskeleton robot considering wearer's condition. *Intell. Serv. Robot.* **2021**, *14*, 345–355.

13. Tanyildizi, A.K.; Yakut, O.; Tasar, B.; Tatar, A.B. Control of twin-double pendulum lower extremity exoskeleton system with fuzzy logic control method. *Neural Comput. Appl.* **2021**, *33*, 8089–8103. [CrossRef]
14. Xie, H.; Xie, Y.; Li, F. The Structure Design and Dynamics Simulation of a New Exoskeleton Robot. In Proceedings of the 2019 WRC Symposium on Advanced Robotics and Automation (WRC SARA), Beijing, China, 21–22 August 2019; IEEE: Piscataway, NJ, USA, 2019; pp. 380–386.
15. Chen, J.; Zhang, X.; Cheng, Y. Surface EMG based continuous estimation of human lower limb joint angles by using deep belief networks. *Biomed. Signal Process. Control* **2018**, *40*, 335–342. [CrossRef]
16. Zhang, Y.N.; Jing, Y.P.; Shen, L.Y.; Song, W.; Qian, J.W. Dimension Reduction and Mapping Analysis of EMG Signals on Lower Limbs. *Chin. J. Sens. Actuators* **2018**, *31*, 1046–1053.
17. Du, Y.; Wang, H.; Qiu, S.; Zhang, J.M.; Xie, P. Continuous Prediction of Joint Angle of Lower Limbs from sEMG Signals. In Proceedings of the 2017 Chinese Intelligent Systems Conference, Xiamen, China, 17–19 November 2017; Springer: Singapore, 2017; pp. 671–679.
18. Gaudet, G.; Raison, M.; Achiche, S. Classification of Upper limb phantom movements in transhumeral amputees using electromyographic and kinematic features. *Eng. Appl. Artif. Intell.* **2018**, *68*, 153–164. [CrossRef]
19. Zheng, W.; Peng, F.; Lan, T. A prosthesis control system based on the combination of speech and sEMG signals and its performance assessment. In Proceedings of the 3rd International Conference on Health Information Science, Shenzhen, China, 22–23 April 2014; Springer International Publishing: Cham, Switzerland, 2014; pp. 72–82.
20. Zhang, T.T.; Fan, Y.B. Motion recognition based on EMG signals of residual limb in transfemoral amputee. *J. Med. Biomech.* **2016**, *31*, 478–482.
21. Sidharth, P.; Amit, M.J. Intelligent upper-limb prosthetic control (iULP) with novel feature extraction method for pattern recognition using EMG. *J. Mech. Med. Biol.* **2021**, *21*, 2150043.
22. Tello, R.M.G.; Filho, T.B.; Neto, A.F.; Arjunan, S.; Kumar, D.K. Feature extraction and classification of sEMG signals applied to a virtual hand prosthesis. In Proceedings of the 2013 35th Annual International Conference of the IEEE Engineering in Medicine and Biology Society, Osaka, Japan, 3–7 July 2013; IEEE: Piscataway, NJ, USA, 2013; pp. 1911–1914.
23. Gao, F.R.; Wang, J.J.; Xi, X.G.; She, Q.S.; Luo, Z.Z. Gait Recognition for Lower Extremity Electromyographic Signals Based on PSO-SVM Method. *J. Electron. Inf. Technol.* **2015**, *37*, 1154–1159.
24. Liu, D.; Zhao, X.G.; Ye, D. SEMG Based Movement Quantitative Estimation of Joins Using SVM Method. In Proceedings of the 19th World Congress of the International Federation of Automatic Control, Cape Town, South Africa, 24–29 August 2014; IFAC: Zürich, Switzerland, 2014; pp. 12311–12316.
25. Dai, H.; Qian, J.W.; Zhang, Z. Application of GRNN in ankle joint motion prediction by EMG signal. *Chin. J. Sci. Instrum.* **2013**, *34*, 845–852.
26. Anwar, T.; Aung, Y.M.; Jumaily, A.A. The estimation of Knee Joint angle based on Generalized Regression Neural Network (GRNN). In Proceedings of the 2015 IEEE International Symposium on Robotics and Intelligent Sensors (IRIS), Langkawi, Malaysia, 18–20 October 2015; IEEE: Piscataway, NJ, USA, 2016.
27. Wang, F.; Yin, T.L.; Lei, C.X.; Zhang, Y.K.; Liu, J. Prediction of lower limb joint angle using sEMG based on GA-GRNN. In Proceedings of the 2015 IEEE International Conference on CYBER Technology in Automation, Control, and Intelligent Systems (CYBER), Shenyang, China, 8–12 June 2015; IEEE: Piscataway, NJ, USA, 2015.